From hexafluorotitanate waste to TiO2 powder: Characterization and evaluation of the influence of synthesis parameters by the experimental design method

Julie Hot, Jérôme Frayret, Vanessa Sonois-Mazars, Erick Ringot

Version of Record: https://www.sciencedirect.com/science/article/pii/S0921883122000498
Manuscript_f4a853f7c15fdf36daf4f4a565795a4a

From hexafluorotitanate waste to TiO_2 powder: characterization and evaluation of the influence of synthesis parameters by the experimental design method

Julie Hot[1]*, Jérôme Frayret[2], Vanessa Sonois-Mazars[1], Erick Ringot[1,3]

[1] LMDC, INSA/UPS Génie Civil, 135 Avenue de Rangueil, 31077 Toulouse Cedex 4 France
[2] INEOSURF, 44 rue Balard, 34790 Grabels France
[3] LRVision SARL, 13 Rue du Développement, 31320 Castanet-Tolosan France
* *Corresponding email: hot@insa-toulouse.fr*

Abstract

This paper was focused on the possible chemical synthesis routes to obtain titanium dioxide, TiO_2, from hexafluorotitanate waste and it was aimed to identify the parameters affecting the formation of crystalline titanium dioxide, TiO_2, phases (anatase or rutile). An experimental design method, inspired from the Taguchi approach, was used to assess the positive or negative impact of input factors on the formation of rutile and anatase, which were the output factors of interest. An experimental matrix was built up with coded values for each factor and coefficients were computed to point out a correlation between outputs and inputs. Particular attention was paid to the chemical compounds (decomplexing agents) added to precipitate TiO_2 from hexafluorotitanates and to the dehydration temperature used to obtain TiO_2 crystallized phases. The powders resulting from the syntheses were investigated by X-Ray diffraction analysis. Their chemical compositions were determined by Inductively Coupled Plasma Atomic Emission Spectroscopy. Data-matching revealed the best synthesis conditions in terms of crystallized TiO_2 content, and this was confirmed by calculating the processing yields. The results showed that silica and calcium hydroxide were the most efficient decomplexing agents leading to the formation of anatase.

Keywords

Titanium dioxide; Hexafluorotitanates; Characterization; Chemical synthesis; Experimental design.

1. Introduction

Titanium dioxide TiO_2 (known as titanium IV oxide or titania) is a naturally occurring white compound created when titanium, one of the most common metals on earth, reacts with the oxygen in the air. It is the most commonly used white pigment and has specific characteristics that make it ideally suited to its many and various applications. For example, it provides whiteness and opacity for paints and coatings, plastics and paper. It is widely used in sun screens because of its UV absorbing properties and its transparency. Moreover, as a photocatalyst, TiO_2 has proved to be useful for a wide variety of environmentally friendly applications, such as microelectronics, solar cells, air and water purification, and has shown self-cleaning and antibacterial properties [1–7]. However, nature does not yield TiO_2 in a form suited to our exploitation of its specific properties. Titanium-containing ores (mainly ilmenite, $FeTiO_3$, but also rutile, which is a naturally occurring TiO_2 mineral) have to be converted into pigment grade TiO_2 by employing either sulfuric acid (sulfate route, mainly ilmenite as feedstock) or chlorine (chloride route, mainly rutile as feedstock), which are the two main production methods [8]. In the sulfate process, ilmenite is digested with concentrated sulfuric acid (H_2SO_4) to form titanyl sulfate ($TiSO_4$), which is converted to hydrated TiO_2 through hydrolysis. In the chlorine process, rutile mineral is reduced with coke and then oxidized at high temperature with gaseous chlorine, which leads to a gas stream containing titanium tetrachloride ($TiCl_4$). This is further purified by distillation and finally reacted with oxygen (in a pure oxygen flame or in plasma) to yield TiO_2 [8,9]. Other methods have been investigated as alternatives [10,11] and further processes are necessary to obtain ultrafine-grade or nanostructured TiO_2 particles, which have a much smaller size distribution than pigmentary particles. Reducing the size of its particles to nanometer scale increases the specific surface of TiO_2 and thus its reactivity [12]. Techniques such as the hydrothermal method, chemical vapor deposition, electro deposition and the sol-gel method are used to obtain nanostructured TiO_2 [13]. They can offer shape and particle size control, which are of the utmost interest if the full potential of TiO_2 is to be exploited. For example, Zhang and Gao obtained rutile titania nanocrystals with rod, sphere and peanut shapes depending on the hydrolytic conditions during hydrothermal

treatment [14]. Wang et al. showed that adding 5% of anatase TiO_2 nanotubes to a Degussa P25 electrode improved the performance of solar cells through better photoelectric properties [15]. Zhou et al. found that the photocatalytic activity was dependent on the surface area and crystallization degree of the anatase particles, which were influenced by the calcination temperature during the hydrothermal method [16]. Moreover, the importance of the calcination process in the formation of nanocrystalline and nanostructured TiO_2, and thus for its performance in various applications, is highlighted in [17–19]. Several TiO_2 synthesis processes, which differ in their chemistry and raw material requirements, are summarized in Table 1.

This paper investigates a way to reclaim TiO_2 from hexafluorotitanate waste coming from chemical milling baths of titanium alloys. This research work was part of the RUTILE project (2016-2019), which is aimed at promoting a circular economy by converting the waste into a compound of interest, TiO_2, and thus reducing waste processing operations. The authors attempted to evaluate the influence of synthesis routes and designed process parameters on the degree of TiO_2 crystallization (anatase and rutile) of the resulting powders. Two input parameters with various levels were investigated: (1) the chemical compounds used as decomplexing agents that were mixed with hexafluorotitanates, and (2) the dehydration temperature. The experimental design method was used to build a matrix with defined, coded values for each level and to compute coefficients to highlight the influence of the input factors. The resulting powders were analyzed through X-Ray Diffraction (XRD), Scanning Electron Microscopy (SEM) and Inductively Coupled Plasma Atomic Emission Spectroscopy (ICP-AES) techniques. The first method allowed the crystallized phases to be identified and the second was used for the quantitative evaluation of chemical elements. The yields (molar ratio between TiO_2 and Ti) of several synthesis processes were then calculated. This approach enabled the final products obtained through the tested syntheses to be compared: it shed light on the importance of the synthesis route used to transform hexafluorotitanates to TiO_2, and pointed to a preferential route for the TiO_2 transformation process.

Table 1. Main TiO_2 synthesis processes reported in the literature.

Initial reagents	Preparation	Heating step	Final compound	Ref.
Ilmenite ($FeTiO_3$, $FeTiO_5$)	Sulfuric acid H_2SO_4 95 %	300 – 500 °C for 10 min – 6 h	Not determined	[20]
Ilmenite ($FeTiO_3$, $FeTiO_5$)	Sulfuric acid H_2SO_4 95 %	180 °C for 5 h	900 °C : Rutile	[21]
Ilmenite ($FeTiO_3$, $FeTiO_5$)	Hydrochloric acid HCl 30 %	25 to 80 °C	600 °C : Rutile	[21]
$TiCl_4$	Reaction with dioxygen O_2	900 to 1600 °C	Rutile	[22]
$TiCl_4$	Reaction with dioxygen O_2	650 to 1800 °C	Rutile	[23]
$Ti(O\text{-}iC_3H_7)_4$	Hydrolyzed by H_2O	85 °C	300 °C: Anatase (6 – 12 nm)	[24]
$TiCl_4$	Hydrolyzed by aqueous ammonium solution NH_3	Room temperature	300 °C: Anatase (6 – 12 nm) 355 °C: Anatase (10 – 15 nm) + trace of rutile	[24]
$TiOSO_4.2H_2O$	Hydrolyzed by aqueous ammonium solution NH_3	Room temperature	300 °C: Anatase (10 – 15 nm) 355 °C: Anatase (10 – 20 nm)	[24]

2. Materials and methods

2.1. Hexafluorotitanates

The Satys ST-Prodem division of the Satys Group, located in Toulouse, France, specializes in the chemical milling of titanium parts for the aerospace industry. Acid baths (a mix of hydrofluoric acid and nitric acid) are used to remove selected areas of a part. As the titanium concentration in the baths increases, anionic titanium fluoride complexes, TiF_6^{2-}, are formed, leading to a decrease in the etching rate. When they become inefficient, the acid baths are wasted and then sent to an appropriate waste facility. In order to reduce the cost of waste management, Satys ST-Prodem has investigated the possibility of restoring the baths by using a chemical reaction based on the addition of sodium salts and has developed a specific regeneration process [25] to precipitate titanium out of chemical baths in the form of sodium hexafluorotitanate compounds (Na_2TiF_6), referred as NTF in this study. The following chemical reactions ((1) to (4)) are involved in the process.

$$2HF + 2NaNO_3 + TiF_4 \leftrightarrows Na_2TiF_6 + 2HNO_3 \quad (1)$$

$$2NaNO_3 + H_2TiF_6 \leftrightarrows Na_2TiF_6 + 2HNO_3 \quad (2)$$

$$2NaF + TiF_4 \leftrightarrows Na_2TiF_6 \quad (3)$$

$$2NaF + H_2TiF_6 \leftrightarrows Na_2TiF_6 + 2HF \quad (4)$$

The NTF precipitate synthesized by Satys ST-Prodem was characterized by ICP-AES in order to detect the presence of impurities. The protocol is described in part 2.4.2 and the results are presented in part 3.1. The theoretical molar mass is $M_{Na2TiF6}$ = 207.8 g/mol. Na_2TiF_6 crystals are soluble in water at a concentration of 65 g/L [21].

2.2. Chemical compounds

The chemical compounds used as decomplexing agents are described in Table 2. Their main role was to promote the NTF to TiO_2 conversion by decomplexing titanium fluorides. Titanium hexafluoride, TiF_6^{2-}, is a preferred product for the synthesis of high purity TiO_2. However, unlike chloride, sulfate and nitrate ions, fluoride ion resists hydrolysis with water, even when it is attempted at the boiling point after dilution. Therefore, it is necessary to add alkali substances to precipitate hydrated TiO_2. Four alkalis were tested in this study: ammonium hydroxide, calcium hydroxide, silica and silicates. Pascal [21] reported that adding ammonium hydroxide (NH_4OH or $NH_3 \bullet H_2O$) to an H_2TiF_6 or Na_2TiF_6 solution resulted in TiO_2 formation. The process takes place in two steps according to reaction (5): first, TiF_4 formation, and then TiO_2 crystallization on exposure to air after boiling. The boiling step allows the excess ammonia and the fluoride ions to be evaporated, thus limiting the formation of oxyfluorotitanate, $TiO_2F_4^{2-}$, in solution, which is as stable as compound TiF_6^{2-}.

$$Na_2TiF_6 + 2NH_4OH + 2OH^- \leftrightarrows 2NH_4F + TiF_4 + 2Na^+ + 4OH^- \xrightarrow{air} TiO_2 + 2F_2 + 2NH_3 + 2F^- + 2Na^+ + 2H_2O \quad (5)$$

The use of an aqueous solution of calcium hydroxide ($Ca(OH)_2$), in which hydroxide ions are available due to the dissociation of $Ca(OH)_2$ electrolyte, also leads to TiO_2 formation according to reaction (6).

However, the compound calcium fluoride (CaF_2) may be found in high proportions in the resulting precipitate.

$$Na_2TiF_6 + 3Ca(OH)_2 \leftrightarrows TiO_2 + 3CaF_2 + 2Na^+ + 2H_2O + 2OH^- \quad (6)$$

The combined use of $NH_3 \bullet H_2O$ and $Ca(OH)_2$ appears to be beneficial to the formation of TiO_2. $Ca(OH)_2$ further increases the pH of the solution due to hydroxide ion addition and reduces the presence of titanium fluoride complexes in the final precipitate. Moreover, calcium ions help to decomplex fluorides from NTF and remove them from the solution through their precipitation into CaF_2 compound, which is more stable (solubility constant: $K_s = 10^{-10.4}$) than TiF_6^{2-} (dissociation constant: $K_d = 10^{-4}$).

Besides ammonium and calcium hydroxides, two other decomplexing agents based on silicon (silica (SiO_2) and silicate (SiO_3^{2-})) were used to promote fluoride exchanges according to reactions (7) and (8). These compounds allow the decomplexation of fluorides from titanium and the complexation of fluorides with silicon. The use of SiO_3^{2-} in liquid form was considered as it could further promote the decomplexation thanks to its increased contact surface with NTF.

$$TiF_6^{2-} + SiO_2 \leftrightarrows TiO_2 + SiF_6^{2-} \quad (7)$$

$$TiF_6^{2-} + SiO_3^{2-} + H_2O \leftrightarrows TiO_2 + SiF_6^{2-} + 2OH^- \quad (8)$$

Reactions (7) and (8) are based on the higher stability of SiF_6^{2-} complex ($K_d = 10^{-10}$) compared to TiF_6^{2-} complex ($K_d = 10^{-4}$). Consequently, SiF_6^{2-} will precipitate with sodium ions present in high proportion in the solution to form Na_2SiF_6 ($K_s = 1.3x10^{-4}$).

Table 2. Chemical compounds used as decomplexing agents.

Decomplexing agent	Chemical formula	Commercial reference
Ammonia	$NH_3 \bullet H_2O$	Solution 25 wt% Labkem
Calcium hydroxide	$Ca(OH)_2$	SLS45, 30 wt%
Silica	SiO_2	Solid particles of SiO_2 180 mesh – 99% - Sigma Aldrich

Silicate	SiO_3^{2-}	Sodium silicate solution 39 wt% Labkem

2.3. Synthesis protocols

The two synthesis routes investigated are illustrated in Fig. 1. They consisted in mixing hexafluorotitanates with a decomplexing agent (cf. Table 2) and water, and bringing the mixture to the boil. Magnetic stirring was carried out at 300 rpm. In the case of route B, $Ca(OH)_2$ was added as a supplementary decomplexing agent and a second boiling step was performed. The pH values of the solutions were between 10 and 11 because the base was in excess. A dehydration step (Nabertherm LE061K17N Muffle furnace) at 400, 550 or 650 °C for 3 h was then conducted on the resulting wet precipitate to obtain the final powders to be analyzed (powders were recovered at ambient temperature, around 25 °C, and thus solubility constants at this temperature were considered). The whole set of experiments is presented in Fig. 2 (a total of 15 syntheses). The final temperature – 400, 550 or 650 °C – was reached after ramping at 15 °C/min. They were carried out under stoichiometric conditions. Data resulting from these experiments were used to relate process factors to final product properties. The objective was to promote the formation of TiO_2 crystallized phases, preferably anatase [26,27].

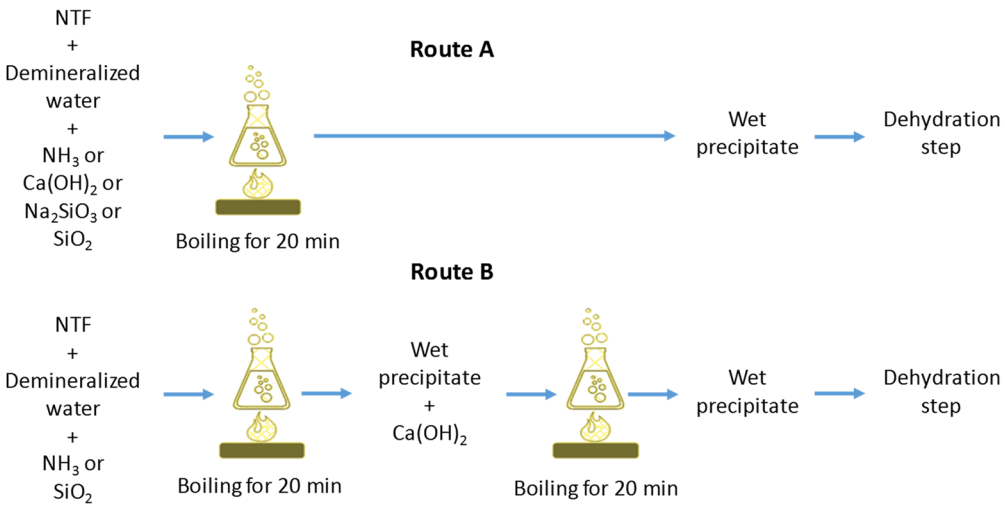

Fig. 1. Synthesis routes A and B. For route A, NTF was mixed with only one decomplexing agent: NH_3, $Ca(OH)_2$, Na_2SiO_3 or SiO_2. Route B used two decomplexing agents: NH_3 or SiO_2, with $Ca(OH)_2$ addition in a second step after a first boiling.

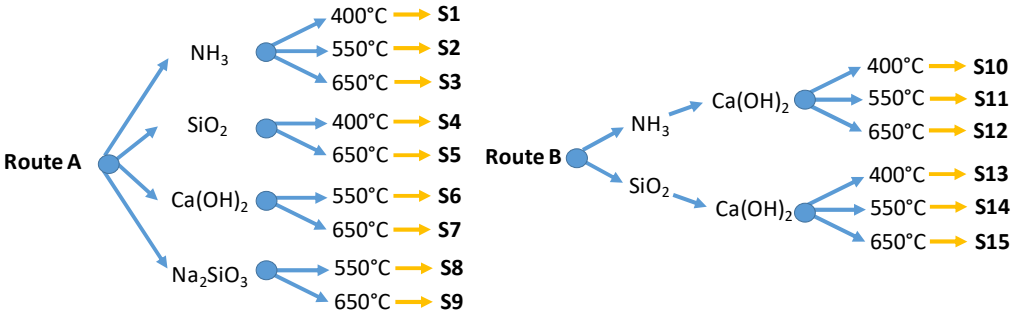

Fig. 2. Schematic representation of the synthesis conditions for routes A and B: decomplexing agents, dehydration temperatures and synthesis numbers.

2.4. Characterization techniques

2.4.1 XRD and SEM/EDS

A Bruker D8 Advance diffractometer was used to identify and compare the crystallized compounds of the synthesized powders. Each of them was homogenized, using ten 6-mm glass balls for 3 minutes, before being ground and sieved with an 80-µm mesh for XRD analyses. This homogenization step allowed segregation of species to be avoided, which was confirmed by the low variability in the diffractograms obtained for three powder samples resulting from the same synthesis. Data collection was carried out at room temperature using Cu K-alpha radiation (λ=1.54 Å). Qualitative identification was conducted with EVA software to collect data necessary for the experimental design method. Anatase and rutile phases exhibited characteristic diffraction peaks at specific 2Θ values: 25.3° (101), 37.3° (004) and 48.0° (200) for anatase, and 27.4° (110), 36.1° (101) and 41.2° (211) for rutile [28,29]. These specific peaks were used to assess the presence of these TiO_2 crystalline forms in the synthesized powders.

Additionally, the microstructure of the synthesized powders was investigated by scanning electron microscopy (SEM). The analyses were conducted with a JEOL KSM 7800F Prime instrument (voltage of 5 and 10 kV). SEM analyses were combined with Energy Dispersive Spectroscopy (EDS) to determine the elementary composition of individual points in the analyzed powders. SEM/EDS allowed the observations resulting from XRD analyses to be corroborated.

2.4.2 ICP-AES

The raw materials and synthesis products were both chemically characterized by ICP-AES. External calibration was used (standard between 0 and 20 mg/L).

For the NTF chemical characterization, the presence of the following elements at specific wavelengths was investigated: Ba (493.408 nm), Cr (205.571 and 206.562 nm), Fe (238.207 and 259.940 nm), Na (589.592 nm), Ni (221.650 and 231.604 nm), S (180.669 nm), Ti (336.122 and 338.377 nm), Zn (206.200 and 213.857 nm) and Zr (343.823 nm). The analyses were carried out in triplicate. Solutions were prepared by diluting between 23 and 55 mg of NTF in 100 ml of demineralized water. They were then diluted 10 times and acidified with a nitric acid solution (HNO_3 2%).

For the chemical characterization of the synthesized powder, the presence of the following elements was investigated at specific wavelengths: Ca (396.847 and 422.673 nm), Na (588.995 and 589.592 nm), Si (251.612 and 288.158 nm) and Ti (334.187 and 334.941 nm). Each synthesized powder was homogenized and milled prior to ICP-AES analysis. Two protocols were used:

- Protocol 1: dissolution of powder (100 mg) in a nitric acid solution (5 ml HNO_3 65%). This protocol allowed the dissolution of sodium, titanium and silicon (added as a decomplexing agent) complexed forms (i.e. containing fluoride) and thus enabled the quantification of Na belonging to Na_2TiF_6, Ti belonging to Na_2TiF_6 and Si belonging to Na_2SiF_6. Only [Si belonging to Na_2SiF_6] is used in the following equations.

- Protocol 2: dissolution of powder (100 mg) in a solution of nitric acid and hydrofluoric acid (2 ml HNO_3 at 65% + 3 ml HF 50%). This protocol led to the dissolution of all sodium, titanium and silicon, including TiO_2 and SiO_2, and thus to the quantification of Na_{Total}, Ti_{Total} and Si_{Total}. Only $[Na_{Total}]$ and $[Ti_{Total}]$ were used for the calculation of $[TiO_2]$ (cf. eq.2).

The concentrations of all chemical species were needed to determine the TiO_2 formed. Its concentration was calculated according to equation 1:

$$[\mathrm{TiO_2}] = [\mathrm{Ti_{Total}}] - [\text{Ti belonging to } \mathrm{Na_2TiF_6}] \quad \text{(eq.1)}$$

$[Ti_{Total}]$ was given by the concentration in Ti obtained with Protocol 2. [Ti belonging to Na_2TiF_6] was determined by the quantification of sodium from Protocol 1. Due to the low solubility of Na_2TiF_6 (K_s = 0.157) and Na_2SiF_6 ($K_s = 1.3 \times 10^{-4}$), sodium mainly precipitated in these two forms (other forms were negligible and NaF was soluble, K_s = 0.97).

Thus:

$$[\text{Na belonging to } \mathrm{Na_2TiF_6}] = [\mathrm{Na_{Total}}] - [\text{Na belonging to } \mathrm{Na_2SiF_6}] \quad \text{(eq.2)}$$

$$[\text{Na belonging to } \mathrm{Na_2SiF_6}] = 2[\text{Si belonging to } \mathrm{Na_2SiF_6}] \quad \text{(eq.3)}$$

And finally:

$$[\mathrm{TiO_2}] = [\mathrm{Ti_{Total}}] - [\text{Na belonging to } \mathrm{Na_2TiF_6}]/2 \quad \text{(eq.4)}$$

$$[\mathrm{TiO_2}] = [\mathrm{Ti_{Total}}] - \left[[\mathrm{Na_{Total}}] - [\text{Na belonging to } \mathrm{Na_2SiF_6}]\right]/2 \quad \text{(eq.5)}$$

$$[\mathrm{TiO_2}] = [\mathrm{Ti_{Total}}] - \left[[\mathrm{Na_{Total}}] - 2[\text{Si belonging to } \mathrm{Na_2SiF_6}]\right]/2 \quad \text{(eq.6)}$$

The quantity of TiO_2 in solution expressed in mol ($nTiO_2$) was calculated using equation 6 and the molar mass of each element: Ti (M_{Ti} = 48 g/mol), Na (M_{Na} = 23 g/mol) and Si (M_{Si} = 28 g/mol). The yield (χ) of a synthesis was then expressed as a percentage according to equation 7.

$$\chi = 100 \times \mathrm{nTiO_2}/\mathrm{nTi_{Total}} \quad \text{(eq.7)}$$

2.4.3 Potentiometry

Fluoride concentration in each NTF sample was determined by potentiometry with the use of an ion-specific electrode for fluoride. This is an electroanalytical method, in which the electrode potential of an electrochemical cell consisting of two electrodes immersed in an electrolyte is measured. The potential that develops across the membrane depends on the difference in the concentration of fluoride ion on either side of the membrane. A fluoride ion selective electrode was used (F-ISE 6.0502.150 Metrohm), in which the sensing element was a crystal membrane of lanthanum fluoride (LaF_3). The reference electrode (LL ISE 6.0750.100, Metrohm) was coated with a thin layer of silver chloride (AgCl). The potentials were measured and the fluoride concentrations were determined for the three NTF samples by using the Nernst equation. OH^- ions have geometry and sizes similar to F^- ions and can therefore interfere with fluoride concentration determination. Measurements were thus carried out at pH 6 to reduce OH^- ion concentration and to avoid the formation of hydrogen fluoride, HF, which would occur for pH below 5.2.

2.5. Experimental design method

The main objective of this research work was to identify the process factors that impact the NTF to TiO_2 conversion, and to find the settings leading to the highest yield. For this purpose, an experimental design method was used, inspired from the Taguchi approach [30,31]. It consisted in analyzing the data resulting from a series of well-defined synthesis processes. Parameters were changed (e.g. decomplexing agent, dehydration temperature) in order to observe the effect the changes had on one or more response factors. The controlled input factors (referred to as IF, from IF1 to IF3) and the measured output factors (referred to as OF, from OF1 to OF3) are shown in Fig. 3. It can be seen that the number of levels of input parameters varied: IF1 had four levels, IF2 had two levels and IF3 had three levels. A coded value from 0 to 3 was attributed to each level as specified in Fig. 3. Results obtained from XRD observations allowed the output responses to be defined (i.e. the

type of crystallized compounds formed for each synthesis tested). The response variable was binary, so two coded values were used: 0 or 1. Value 1 meant that a crystallized compound (anatase, rutile or Na_3TiOF_5) was detected in the synthesized powders. Otherwise, value 0 was attributed. The coded values associated with input and output factors were used to build an experimental matrix, a schematic representation of which is shown in Table 3.

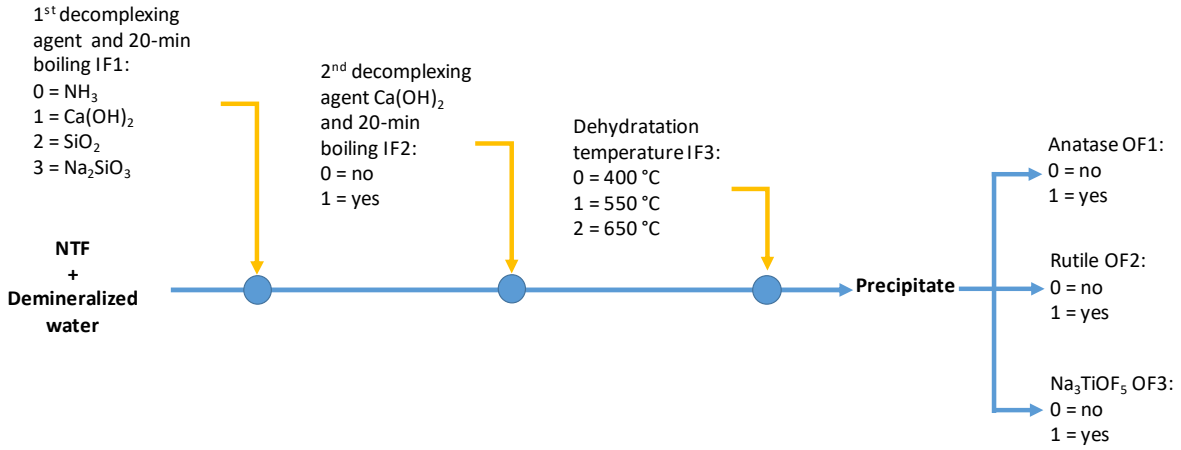

Fig. 3. Input and output factors (IF and OF) identified for the experimental design method. Three input factors were considered, each of them having various levels: IF1 had four levels, IF2 had two levels and IF3 had three levels. A coded value (0, 1, 2 or 3) was attributed to each level. Output response was binary (0 or 1).

Table 3. Schematic representation of the experimental matrix with coded values $X_{i/k}$ and $Y_{j/k}$ for each factor (IF = input factor, OF = output factor). Letters i, j and k refer to the input factor number ($1 \leq i \leq 3$), output factor number ($1 \leq j \leq 3$) and synthesis number ($1 \leq k \leq 15$) respectively. $X_{i/k}$ = 0, 1, 2 or 3 and $Y_{j/k}$ = 0 or 1 according to Fig. 2 and 3.

Factor/Synthesis	IF1	IF2	IF3	OF1	OF2	OF3
S1	$X_{1/1}$	$X_{2/1}$	$X_{3/1}$	$Y_{1/1}$	$Y_{2/1}$	$Y_{3/1}$
.	.	.	.	.	.	.
.	.	.	.	.	.	.
.	.	.	.	.	.	.
S15	$X_{1/15}$	$X_{2/15}$	$X_{3/15}$	$Y_{1/15}$	$Y_{2/15}$	$Y_{3/15}$

The influence of the levels of each input factor on the formation of anatase (OF1), rutile (OF2) and Na_3TiOF_5 (OF3) was then assessed. Equation 8 was used to calculate the coefficient for each level of

each input factor and point out a correlation between output and input factors. For this purpose, the binary quantity $\mathrm{Z_{i/k}}(L)$ was introduced as $\mathrm{Z_{i/k}}(L) = 1\ if\ \mathrm{X_{i/k}} = L\ else\ \mathrm{Z_{i/k}}(L) = 0$. The coupling between the input factors was not taken into account. Therefore:

$$\mathrm{C^{j}_{i}(L)} = \frac{1}{\mathrm{n}}\sum_{\mathrm{k}} \mathrm{Z_{i/k}\,(L)} \times\ \mathrm{Y_{j/k}} \qquad \text{(eq.8)}$$

In this expression, the notations i, j, k and L respectively refer to the input factor number $1 \leq i \leq 3$, the output factor number $1 \leq j \leq 3$, the synthesis index $1 \leq k \leq 15$ and the factor level index $0 \leq L \leq 3$. The letter n stands for the number of occurrences of L in the column $\left|\mathrm{X_{i/k}}\right|$. A matrix of computed coefficients $\mathrm{C^{j}_{i}(L)}$ like the one shown in Table 4 was obtained for each output factor studied (3 matrices were obtained).

Table 4. Example of a matrix of computed coefficients $C^{j}_{i}(L)$ obtained for an output factor j (1≤j≤3). Each coefficient indicates the influence of the level L (1≤L≤3) of each input factor i (1≤i≤3) on the output factor j.

Factor/Level	IF1	IF2	IF3
0	$C^{j}_{1}(0)$	$C^{j}_{2}(0)$	$C^{j}_{3}(0)$
1	$C^{j}_{1}(1)$	$C^{j}_{2}(1)$	$C^{j}_{3}(1)$
2	$C^{j}_{1}(2)$	/	$C^{j}_{3}(2)$
3	$C^{j}_{1}(3)$	/	/

3. Results

3.1. NTF chemical composition

Quantities (in grams) of titanium, sodium and fluoride for three NTF samples are shown in Table 5. Only titanium and sodium were measured by ICP-AES. The other elements investigated were below the detection limit (0.005 wt% of the sample). The fluoride quantities were deduced by potentiometry from concentration measurements. This analysis shows that sodium hexafluorotitanate compounds resulting from the Satys ST-Prodem regeneration process were

composed of sodium, titanium and fluoride (Na_2TiF_6) for 93 ± 2 wt%. The non-identified compounds might be water or other chemical residues from the baths.

Table 5. Titanium, sodium (ICP-AES) and fluoride (potentiometry) quantities (in grams) for three NTF samples and Na_2TiF_6/NTF ratio values.

Sample	m_{NTF} analyzed (g)	mNa (g)	mTi (g)	mF (g)	$m_{Na2TiF6}$ measured (g)	% Na_2TiF_6/NTF
Sample 1	0.0230	0.0045	0.0049	0.0114	0.0208	90.4
Sample 2	0.0340	0.0068	0.0072	0.0182	0.0323	94.8
Sample 3	0.0555	0.0107	0.0118	0.0291	0.0516	93.7

3.2. Crystallized phases observed by XRD and SEM/EDS

Table 6 reports the phases detected by XRD for each synthesized powder. They varied depending on the decomplexing agents used and the dehydration temperature. The crystallized phases of interest for this study were anatase, rutile and Na_3TiOF_5. The first two were chosen because they showed which synthesis conditions promoted the conversion of NTF to TiO_2 and the third one because it provided information on the conditions to be avoided because they led to the formation of $TiO_xF_y^{(4-y-2x)}$ complexed forms. As an example, the diffractogram of the powder obtained from synthesis S15 is illustrated in Fig. 4. The main peaks of the compounds identified (anatase, rutile, NaF, CaF_2, SiO_2) are shown. Moreover, the residual compound Na_3AlF_6, known as cryolite, was detected. Acid baths were used for the chemical milling of titanium alloys containing from 5.5 to 6.5 % of aluminum, which, by forming complexes with fluorides in the baths, can precipitate throughout the NTF synthesis.

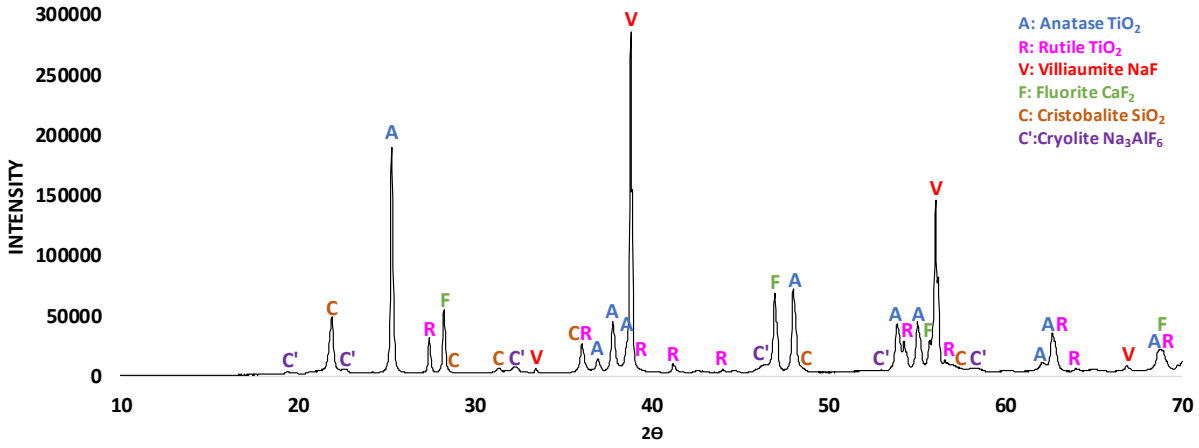

Fig. 4. Diffractogram of the powder obtained from synthesis S15 (SiO_2 + $Ca(OH)_2$ at 650 °C).

Table 6. Crystallized phases detected by XRD for each synthesis.

Synthesis	Crystallized TiO_2 phase	Other crystallized phase
S1	Anatase	Na_3TiF_6
S2	Rutile	Na_3TiOF_5
S3	Rutile	Na_3TiOF_5
S4	Anatase	Na_3TiOF_5 + Na_3TiF_6+ Na_2SiF_6 + SiO_2
S5	Anatase + Rutile	Na_3TiOF_5 + NaF + SiO_2
S6	Rutile	Na_3TiOF_5 + CaF_2 + $CaSO_4$, $0,5H_2O$
S7	Rutile	Na_3TiOF_5 + CaF_2 + $CaSO_4$, $0,5H_2O$
S8	Anatase	Na_3TiOF_5
S9	Anatase	Na_3TiOF_5
S10	Anatase	Na_3TiOF_5 + CaF_2 + Na_3TiF_6
S11	Rutile	Na_3TiOF_5 + Na_2TiF_6+ CaF_2
S12	Rutile	Na_3TiOF_5 + CaF_2
S13	Anatase	Na_3TiOF_5 + Na_3TiF_6+ CaF_2 + SiO_2
S14	Anatase+ Rutile	Na_3TiOF_5 + CaF_2 + SiO_2
S15	Anatase+ Rutile	NaF + CaF_2 + SiO_2

Fig. 5 also shows several SEM images of the powder obtained from synthesis S15. EDS analyses combined with XRD results allowed the compounds specified in this figure to be identified (cf. Fig. S1 provided in Supplementary Information). Silica SiO_2 particles, added during the synthesis as decomplexing agent, are observed in Fig. 5.b, and sodium fluoride NaF and calcium fluoride CaF_2 can be seen in Figs. 5.d and 5.e, respectively. Finally, the expected TiO_2 crystallized phases, anatase and

rutile, were identified, as shown in Fig. 5.f. The more elongated shapes were associated with rutile particles and the shorter, cubic ones - with the anatase particles [32,33]. Further details were reported by the authors in a previous paper [34].

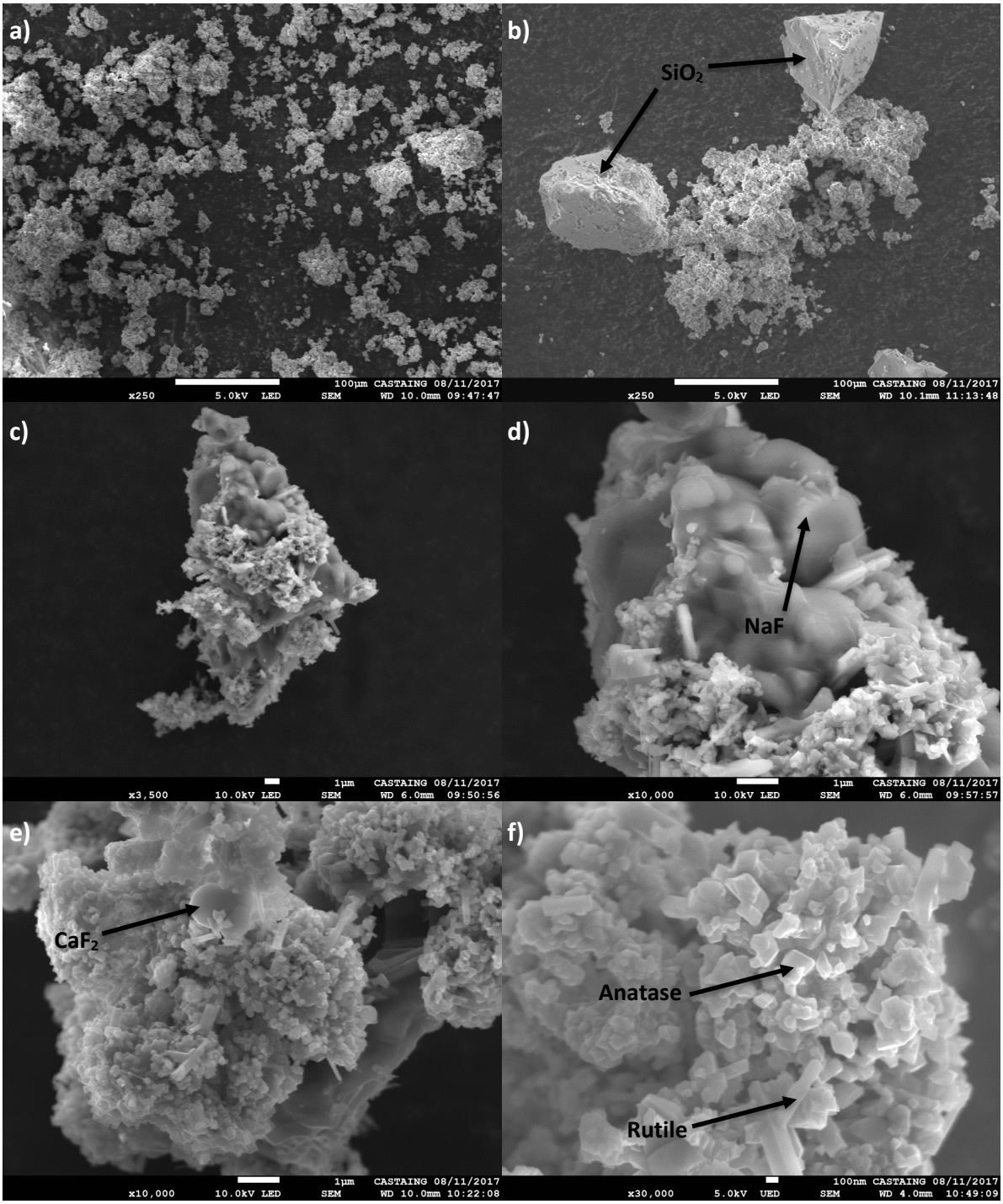

Fig. 5. SEM images of the powder obtained from synthesis S15: a) and b) magnification x250, c) magnification x3 500, d) and e) magnification x10 000, f) magnification x30 000. The compounds detected by XRD were observed: SiO_2, NaF, CaF_2, anatase (cubic form) and rutile (stick form).

3.3. Experimental matrix and computed coefficients

Table 7 shows the final experimental matrix (the first-order interactions are not shown). As explained in part 2.5, a coded value between 0 and 3 was associated with each level of input factors. The response variable was binary: the coded value 0 or 1 was attributed according to XRD observations (cf. Table 6). It can be seen that anatase (OF1) or rutile (OF2) phases were detected in each powder (coded value 1) and both of these phases were observed in powders resulting from syntheses 5, 14 and 15. For Na_3TiOF_5 (OF3), only syntheses 1 and 15 did not lead to its formation (coded value 0).

In order to further analyze this experimental matrix and link inputs to outputs, coefficients were computed by using equation 8. The results are presented in Table 8. A coefficient was obtained for each level to assess its impact on each output factor: the higher the coefficient, the greater its contribution.

Table 7. Experimental matrix containing the coded values defined for input factors (IF) and output factors (OF).

Synthesis	IF1	IF2	IF3	OF1 Anatase	OF2 Rutile	OF3 Na_3TiOF_5
S1	0	0	0	1	0	0
S2	0	0	1	0	1	1
S3	0	0	2	0	1	1
S4	2	0	0	1	0	1
S5	2	0	2	1	1	1
S6	1	0	1	0	1	1
S7	1	0	2	0	1	1
S8	3	0	1	1	0	1
S9	3	0	2	1	0	1
S10	0	1	0	1	0	1
S11	0	1	1	0	1	1

S12	0	1	2	0	1	1
S13	2	1	0	1	0	1
S14	2	1	1	1	1	1
S15	2	1	2	1	1	0

Table 8. Computed coefficients. Each coefficient indicates the influence of the level of each input factor (IF1, IF2, and IF3) on the output factors (OF1, OF2 and OF3). The highest values are in bold.

OF1 Anatase			
Factor/ Level	IF1	IF2	IF3
0	0.33	0.56	**1.00**
1	0.00	**0.67**	0.40
2	**1.00**		0.50
3	**1.00**		
OF2 Rutile			
Factor/ Level	IF1	IF2	IF3
0	0.67	0.56	0.00
1	**1.00**	**0.67**	0.80
2	0.60		**0.83**
3	0.00		
OF3 Na_3TiOF_5			
Factor/ Level	IF1	IF2	IF3
0	0.83	0.89	0.75
1	**1.00**	**1.00**	**1.00**
2	0.80		0.83
3	**1.00**		

3.4. Chemical compositions of the synthesized powders and yield values

The chemical compositions of ten synthesized powders obtained by ICP-AES analyses and their yield values are shown in Table 9 (only the best syntheses were considered). The yield (χ) was calculated using equation 7. It was defined as the ratio between TiO_2 quantity and Ti quantity measured by ICP-

AES. The values obtained varied between 25 and 120%. Uncertainties in sample preparation procedure and measurement were responsible for the yield values above 100% (uncertainty was estimated to be ± 5% for Na and Ti, and ± 10% for Si). As will be discussed in the following part, yield results were used to identify the best experimental settings, which led to the highest TiO_2 formation from titanium contained in NTF. In the case of syntheses S8 and S9, the yield values were corrected to take the overestimation into account for [Si belonging to Na_2SiF_6] obtained by ICP-AES from Protocol 1 through the addition of Na_2SiO_3 as a decomplexing agent (high solubility of SiO_3^{2-}).

Table 9. Chemical compositions obtained by ICP-AES analyses and yields of synthesized powders. nTi total in mol, $nTiO_2$ in mol and yield χ in percentage are calculated using the molar mass of Ti, eq.6 and eq.7 (* corrected value).

Synthesis	Na total (wt%)	Ti total (wt%)	Si belonging to Na_2SiF_6 (wt%)	nTi total (mol)	$nTiO_2$ (mol)	Yield χ (%)
S2	14.73	20.61	0.00	0.43	0.11	25
S3	12.67	20.87	0.00	0.43	0.16	37
S6	13.92	19.80	0.06	0.41	0.11	27
S7	8.87	15.45	1.43	0.32	0.18	56
S8	6.44	8.98	7.27	0.19	0.31	114*
S9	11.84	6.99	10.94	0.15	0.28	111*
S11	12.87	19.02	0.40	0.40	0.13	33
S12	10.73	18.42	0.00	0.38	0.15	39
S13	8.63	11.90	4.92	0.25	0.24	95
S14	8.79	15.31	6.12	0.32	0.35	108
S15	8.57	14.05	6.84	0.29	0.35	120

4. Discussion

The contribution of each input factor level on OF1, OF2 and OF3 was assessed by comparing the coefficient values summarized in Table 8. A schematic representation is shown in Fig. 6. Several trends were drawn from these results. We focus on the highest coefficients obtained for IF1, IF2 and IF3.

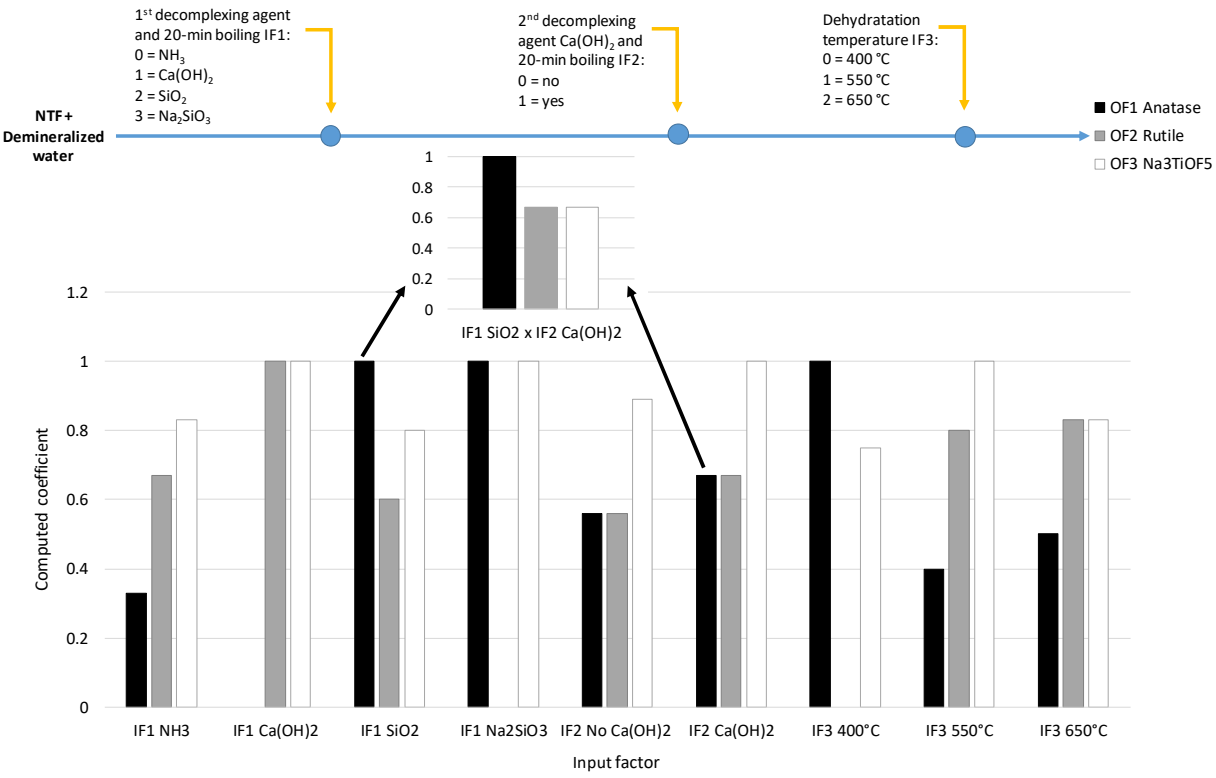

Fig. 6. Schematic representation of the influence of the level of each input factor (IF1, IF2 and IF3) on output factors (OF1, OF2 and OF3). Results of the first-order interaction IF1xIF2 are shown.

The results obtained for input factors IF1 highlighted the role played by the nature of the decomplexing agent. In the case of OF1 (anatase formation), a coefficient of 1 was obtained for levels 2 and 3 of IF1, which means that the use of silica (SiO_2) or silicate (SiO_3^{2-}) as the decomplexing agent favored the formation of anatase. In the case of OF2 (rutile formation), adding calcium hydroxide at the first step (level 1 of IF1) had a positive effect, as the computed coefficient was 1. In addition, it can be noted that the use of ammonium hydroxide tended to favor rutile rather than anatase phase (0.67 vs. 0.33). As previously explained, calcium hydroxide and silicon-based agents were used to increase the pH so as to free fluorides and thus promote their decomplexation from NTF by forming CaF_2 compound or SiF_6^{2-}complex. Concerning oxyfluorotitanate Na_3TiOF_5, it was difficult to identify the influence of the decomplexing agents on its formation (computed coefficient values were above 0.80). This crystallized phase was an expected intermediate product of the transformation of NTF and was qualitatively detected by XRD analyses in most syntheses (cf. Table 6).

A first-order interaction study, i.e. between two factors, was carried out to highlight the interaction between the first decomplexing agent (IF1) and the $Ca(OH)_2$ added as a second decomplexing agent (IF2). The columns of the first-order interactions were obtained by a point to point product of the columns of the coded values of IF1 and IF2. It was observed that the combined use of SiO_2 and $Ca(OH)_2$ favored the formation of anatase (computed coefficient = 1) rather than rutile or Na_3TiOF_5 phases (both computed coefficients = 0.67). The positive effect on anatase formation of using SiO_2 could be explained by the influence of particle size during treatment. This aspect is notably discussed by Ovenstone and Yanagisawa in [35]. The smaller the crystallite size, the higher the proportion of rutile phase after calcination. They explain that powders with very small crystallite sizes contain a larger number of lattice defects, in which the atoms have a higher energy and act as nucleation sites for the formation of rutile at the surface of the crystallites. The addition of $Ca(OH)_2$ allowed an increase in pH, which further promoted the formation of anatase [35,36].

The results for input factor IF3 highlighted the effect of the dehydration temperature. The computed coefficients showed that conducting the dehydration at a high temperature (650 °C, level 3 of IF3) promoted the formation of rutile phase (computed coefficient = 0.83), while anatase phase was observed under lower temperature (400 °C, level 0 of IF3, computed coefficient = 1). The literature on the anatase to rutile transition temperature seems to converge on a value around 600 °C. The effect of calcination temperature on crystal structure of TiO_2 powders was reported by Wetchakun et al. [17]. The authors observed a decrease in the anatase phase composition with increasing calcination temperatures, the anatase to rutile phase transition occurring at 500-600 °C. This phenomenon was also highlighted by Matthews, who observed the apparition of rutile during the hydrothermal crystallization of amorphous titanium dioxide at 600 °C [36]. The transformation of anatase to rutile is based on a nucleation-growth process: the anatase nucleates first and the rutile phase forms later when there is a sufficient surface of anatase available to spread into [36,37]. This process is greatly influenced by the kinetics of processing methods and the presence of impurities and doping ions. It can occur at lower or higher temperature, from 400 °C to 1200 °C [37,38]. In a

previous paper, the authors notably showed that, for the same raw materials, the anatase to rutile transition tended to occur between 400 °C and 550 °C [34]. Moreover, the computed coefficients obtained for OF3 did not clearly identify an effect of the temperature on the formation of Na_3TiOF_5. Borowiec et al. studied the kinetics of the oxidation of sodium fluorotitanates Na_2TiF_6 and Na_3TiF_6, for which Na_3TiOF_5 was an intermediate product [39]. They showed that the oxidation of Na_3TiOF_5 from Na_2TiF_6 reactant started to occur at around 600 °C and continued up to 800 °C as the final product – a mixture of NaF and TiO_2 – could not coexist at high temperature (above 800 °C). The dehydration temperatures tested in this study were probably too low to allow total oxidation of Na_3TiOF_5.

The above analyses of the computed coefficients (cf. Table 8) are consistent with the yield values reported in Table 9. Syntheses S8, S9, S13, S14 and S15 gave the highest yields: 114, 111, 95, 118 and 120% respectively, which means that the initial Ti content (in the NTF) was totally converted into TiO_2 (crystallized and amorphous phases). In addition, these high yield values imply that the quantity of Na_3TiOF_5 phase formed during these syntheses was minor.

In the authors' opinion, the synthesis route with silica and calcium hydroxide under a suitable dehydration temperature should be preferred to promote anatase formation from NTF as these substances are easy to handle. In addition, as these reactants are safe, cheap and widely used, the process could be considered at the industrial scale.

5. Conclusion

The research work presented in this paper focused on the influence of synthesis parameters on the transformation of hexafluorotinates (NTF) to titanium dioxide. It highlighted the importance of the synthesis route. The aim of this study was to find the best experimental setting to obtain TiO_2 from an industrial waste. For this purpose, an experimental design method was used to collect a maximum of information while carrying out a limited number of experiments. Various synthesis routes were investigated with the aim of promoting the formation of crystallized TiO_2 phases, preferentially

anatase. The synthesized powders were then chemically characterized. Data collection from XRD analyses helped to build an experimental matrix by identifying the output factors, the input factors being defined depending on the synthesis parameters. Response coefficients were computed to assess the positive or negative impact of the decomplexing agent and dehydration temperature on the formation of anatase, rutile and sodium oxyfluorotitanate. TiO_2 crystallized phases were observed in all powders synthesized. However, computed coefficients showed that the combined use of SiO_2 and $Ca(OH)_2$ promoted anatase formation, which was preferably obtained under lower dehydration temperature. Moreover, the SiO_2 allowed powders to be synthesized with larger crystallite sizes, leading to a higher proportion of anatase. Also, such decomplexing agents – silica and calcium hydroxide – could be safely used at the industrial scale. Further research needs to be carried out to optimize the dehydration step (temperature and time) so as to increase anatase content. Synthesized TiO_2 powders could be put to valuable use in other industries (e.g. photocatalytic coating for air-depollution or self-cleaning applications).

Acknowledgments

This research work (RUTILE project, EASYNOV Eco-innovation 2016, 2016-2019) was supported by the Occitanie Region and the European Regional Development Fund (cf. Fig. 7). The authors are grateful to Satys ST-Prodem for its collaboration (in particular via Mr. Mathieu Nicolas).

Fig. 7. European Union and Occitanie Region logos ("Project co-funded by the European Regional Development Fund").

References

[1] A. Fujishima, X. Zhang, Titanium dioxide photocatalysis: present situation and future approaches, Comptes Rendus Chimie. 9 (2006) 750–760. https://doi.org/10.1016/j.crci.2005.02.055.

[2] J. Ângelo, L. Andrade, L.M. Madeira, A. Mendes, An overview of photocatalysis phenomena applied to NOx abatement, Journal of Environmental Management. 129 (2013) 522–539. https://doi.org/10.1016/j.jenvman.2013.08.006.

[3] T. Verdier, M. Coutand, A. Bertron, C. Roques, Antibacterial activity of TiO2 photocatalyst alone or in coatings on E. coli: The influence of methodological aspects, Coatings. 4 (2014) 670–686. https://doi.org/10.3390/coatings4030670.

[4] V.N. Kruchinin, T.V. Perevalov, V.V. Atuchin, V.A. Gritsenko, A.I. Komonov, I.V. Korolkov, L.D. Pokrovsky, C.W. Shih, A. Chin, Optical Properties of TiO2 Films Deposited by Reactive Electron Beam Sputtering, Journal of Electronic Materials. 46 (2017) 6089–6095. https://doi.org/10.1007/s11664-017-5552-3.

[5] J.S. Pozo-Antonio, A. Dionísio, Self-cleaning property of mortars with TiO2 addition using real diesel exhaust soot, Journal of Cleaner Production. 161 (2017) 850–859. https://doi.org/10.1016/j.jclepro.2017.05.202.

[6] V.M. Kalygina, I.S. Egorova, I.A. Prudaev, O.P. Tolbanov, V.V. Atuchin, Conduction mechanism of metal-TiO2–Si structures, Chinese Journal of Physics. 55 (2017) 59–63. https://doi.org/10.1016/j.cjph.2016.08.011.

[7] L. Dyshlyuk, O. Babich, S. Ivanova, N. Vasilchenco, V. Atuchin, I. Korolkov, D. Russakov, A. Prosekov, Antimicrobial potential of ZnO, TiO2 and SiO2 nanoparticles in protecting building materials from biodegradation, International Biodeterioration & Biodegradation. 146 (2020) 104821. https://doi.org/10.1016/j.ibiod.2019.104821.

[8] M.J. Gázquez, J.P. Bolívar, R. Garcia-Tenorio, F. Vaca, A review of the production cycle of titanium dioxide pigment, Materials Sciences and Applications. 2014 (2014). https://doi.org/10.4236/msa.2014.57048.

[9] E. Reck, M. Richards, TiO2 manufacture and life cycle analysis, Pigment & Resin Technology. 28 (1999) 149–157. https://doi.org/10.1108/03699429910271297.

[10] S. Middlemas, Z.Z. Fang, P. Fan, A new method for production of titanium dioxide pigment, Hydrometallurgy. 131–132 (2013) 107–113. https://doi.org/10.1016/j.hydromet.2012.11.002.

[11] W.P.C. Duyvesteyn, B.J. Huls, P.L. Shrestha, Processing ilmenite ore to TiO2 pigment, WO1996024555A1, 1996.

[12] K. Suttiponparnit, J. Jiang, M. Sahu, S. Suvachittanont, T. Charinpanitkul, P. Biswas, Role of surface area, primary particle size, and crystal phase on titanium dioxide nanoparticle dispersion properties, Nanoscale Research Letter. 6 (2010) 27. https://doi.org/10.1007/s11671-010-9772-1.

[13] M.M. Byranvand, A.N. Kharat, L. Fatholahi, Z.M. Beiranvand, A Review on Synthesis of Nano-TiO2 via Different Methods, Journal of Nanostructures. 3 (2013) 1–9. https://doi.org/10.7508/jns.2013.01.001.

[14] Q. Zhang, L. Gao, Preparation of oxide nanocrystals with tunable morphologies by the moderate hydrothermal method: Insights from rutile TiO2, Langmuir. 19 (2003) 967–971. https://doi.org/10.1021/la020310q.

[15] Y. Zhou, Y. Huang, D. Li, W. He, Three-dimensional sea-urchin-like hierarchical TiO2 microspheres synthesized by a one-pot hydrothermal method and their enhanced photocatalytic activity, Materials Research Bulletin. 48 (2013) 2420–2425. https://doi.org/10.1016/j.materresbull.2013.02.051.

[16] D. Wang, B. Yu, F. Zhou, C. Wang, W. Liu, Synthesis and characterization of anatase TiO2 nanotubes and their use in dye-sensitized solar cells, Materials Chemistry and Physics. 113 (2009) 602–606. https://doi.org/10.1016/j.matchemphys.2008.08.011.

[17] N. Wetchakun, B. Incessungvorn, K. Wetchakun, S. Phanichphant, Influence of calcination temperature on anatase to rutile phase transformation in TiO2 nanoparticles synthesized by

the modified sol–gel method, Materials Letters. 82 (2012) 195–198. https://doi.org/10.1016/j.matlet.2012.05.092.

[18] G. Liu, X. Yan, Z. Chen, X. Wang, L. Wang, G.Q. Lu, H.-M. Cheng, Synthesis of rutile–anatase core–shell structured TiO2 for photocatalysis, Journal of Materials Chemistry. 19 (2009) 6590–6596. https://doi.org/10.1039/B902666E.

[19] W. Zhang, H. Tang, Rutile nanopowders for pigment production: Formation mechanism and particle size prediction, Chemical Physics Letters. 692 (2018) 129–133. https://doi.org/10.1016/j.cplett.2017.12.025.

[20] P.D. Thometzek, G.D. Linde, Verfahren zur Herstellung von Titandioxid nach dem Sulfatverfahren - Process for the preparation of titanium dioxide by the sulphate process, EP0659688A1, 1995.

[21] P. Pascal, P. Albert, Nouveau Traité de Chimie Minérale, Tome IX, Titane, Zirconium, Hafnium, Thorium, Paris. (1963).

[22] J.C. Deberry, M. Robinson, M.D. Pomponi, A.J. Beach, Y. Xiong, K. Akhtar, Controlled vapor phase oxidation of titanium tetrachloride to manufacture titanium dioxide, US6387347B1, 2002.

[23] N.S. Subramanian, R.P. Bernard, Y.-H.S. Hsu, C.D. Musick, K. Ogunde, J.N. Tilton, Process for producing titanium dioxide, US7476378B2, 2009.

[24] Y. Suwa, M. Inagaki, S. Naka, Polymorphic transformation of titanium dioxide by mechanical grinding, Journal of Materials Science. 19 (1984) 1397–1405. https://doi.org/10.1007/BF00563034.

[25] M. Nicolas, Procédé de régénération d'un bain d'usinage chimique de pièces en titane, WO2018229672A1, 2018.

[26] T. Luttrell, S. Halpegamage, J. Tao, A. Kramer, E. Sutter, M. Batzill, Why is anatase a better photocatalyst than rutile? - Model studies on epitaxial TiO2 films, Scientific Reports. 4 (2014) 1–8. https://doi.org/10.1038/srep04043.

[27] L. Liu, H. Zhao, J.M. Andino, Y. Li, Photocatalytic CO2 reduction with H2O on TiO2 nanocrystals: Comparison of anatase, rutile, and brookite polymorphs and exploration of surface chemistry, ACS Catalysis. 2 (2012) 1817–1828. https://doi.org/10.1021/cs300273q.

[28] D.A.H. Hanaor, C.C. Sorrell, Review of the anatase to rutile phase transformation, Journal of Materials Science. 46 (2011) 855–874. https://doi.org/10.1007/s10853-010-5113-0.

[29] R.R. Guimaraes, A.L.A. Parussulo, K. Araki, Impact of nanoparticles preparation method on the synergic effect in anatase/rutile mixtures, Electrochimica Acta. 222 (2016) 1378–1386. https://doi.org/10.1016/j.electacta.2016.11.114.

[30] P. Alexis, Cours de plan d'expérience (sous forme littérale), (2015). https://docplayer.fr/46169131-Cours-de-plan-d-experience-sous-forme-litterale.html (accessed April 8, 2020).

[31] J. Goupy, Les plans d'expériences - Optimisation du choix des essais et de l'interprétation des résultats, 5ème édition, Librairie Eyrolles, 2017.

[32] T. Ohno, K. Sarukawa, M. Matsumura, Crystal faces of rutile and anatase TiO2 particles and their roles in photocatalytic reactions, New Journal of Chemistry. 26 (2002) 1167–1170. https://doi.org/10.1039/B202140D.

[33] T. Taguchi, Y. Saito, K. Sarukawa, T. Ohno, M. Matsumura, Formation of new crystal faces on TiO2 particles by treatment with aqueous HF solution or hot sulfuric acid, New Journal of Chemistry. 27 (2003) 1304–1306. https://doi.org/10.1039/B304518H.

[34] J. Hot, A. Dasque, J. Topalov, V. Mazars, E. Ringot, Titanium valorization: From chemical milling baths to air depollution applications, Journal of Cleaner Production. 249 (2020) 119344. https://doi.org/10.1016/j.jclepro.2019.119344.

[35] J. Ovenstone, K. Yanagisawa, Effect of hydrothermal treatment of amorphous titania on the phase change from anatase to rutile during calcination, Chemistry of Materials. 11 (1999) 2770–2774. https://doi.org/10.1021/cm990172z.

[36] A. Matthews, The crystallization of anatase and rutile from amorphous titanium dioxide under hydrothermal conditions, American Mineralogist. 61 (1976) 419–424.

[37] R.D. Shannon, J.A. Pask, Kinetics of the anatase-rutile transformation, Journal of the American Ceramic Society. 48 (1965) 391–398. https://doi.org/10.1111/j.1151-2916.1965.tb14774.x.

[38] J.C. Jamieson, B. Olinger, Pressure-temperature studies of anatase, brookite rutile, and TiO2(II): A discussion, American Mineralogist. 54 (1969) 1477–1481.

[39] K. Borowiec, A. Przepiera, K. Kolbrecka, Intrinsic kinetics of the oxidation of Na2TiF6 and Na3TiF6, Journal of Thermal Analysis and Calorimetry. 37 (1991) 637–644. https://doi.org/10.1007/BF01913115.

Hexafluorotitanate compound: a waste coming from chemical milling baths of titanium alloys

Syntheses: various decomplexing agents and dehydration temperatures

Synthesized powders: characterization by XRD, SEM/EDS, and ICP analyses

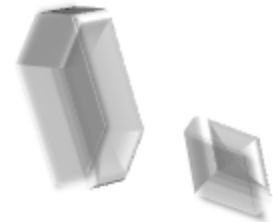

TiO_2 crystallized phases: anatase and rutile

Experimental design method